

Sonar Image Registration and Mosaic Based on Line Detection and Triangle Matching

LIU Tao, ZHANG Xuguang, WANG Yuxi, FANG Yinfeng, GUO Chunsheng

(School of Communication Engineering, Hangzhou Dianzi University, Hangzhou, China)

Abstract: Image registration is an important research topic in the field of computer vision, in which the registration and mosaic of side-scan sonar images is the keypoints of underwater navigation. However, the image registration method of keypoints is not suitable for sonar images which do not have obvious feature points. Therefore, a method of sonar-image registration and mosaic based on line segment extraction and triangle matching is proposed in this paper. Firstly, in order to extract features from sonar image, the LSD method is introduced to detect line feature from images, and line segments are filtered by the principle of attention; after that, triangles are formed from line segments, an image transformation matrix can be calculated through the heuristic greedy algorithm from these triangles; finally, images are merged based on the transformation information. On the basis of practical tests, it is found that, the feature extraction method used in this paper can better describe the outline of underwater terrain, and there is no obvious stitching gap between the result of sonar images stitched. Experimental results show that the proposed method is effective than the keypoints method of the registration and mosaic of sonar images.

Key words: Sonar Image, Image Registration, Line Segment Detector, Triangle Matching

1 Introduction

Sonar image processing is an important component of underwater signal processing technology and it has been applied to many fields, such as underwater navigation^[1-4], marine life analysis^[5-6], underwater terrain analysis^[7-8] and target detection^[9-13]. Image registration transforms two or more images from different time, different sensors, different perspectives to the same coordinate system to obtain the transform matrix for matching and stacking^[14]. There are three kinds of image registration methods, gray level information, transformation domain and feature-based methods. The following are the application of these three methods respectively. D. I. Barnea and H.F. Silverman presents a fast region matching algorithm based on

gray information, which uses sequence similarity detection as a similarity measurement function^[15]. On the basis of ensuring matching accuracy, this method effectively reduces the amount of computation, which can improve the matching speed. However, the error threshold needs to be set in the calculation, so it is crucial to choose a suitable threshold. P.E. Anuta presents an image registration method using FFT phase invariance transform domain information^[16]. This algorithm is easy to implement in code, but it can only accurately match the case of translation, and cannot match the case of rotation and scaling. Neto.V.F.D.C and Campos M.F.M presents a novel methodology to perform matching between image points described by their respective features^[17]. This algorithm has low computational complexity and strong robustness,

but it can easily cause mismatches by extracting too many keypoints, and the calculation time of this algorithm is too long to meet the real-time requirements.

Feature extraction is crucial for image recognition, and proper feature extraction is helpful for the subsequent detection and recognition [18]. Feature-based registration method is widely used in many fields [19-21]. This kind of methods can be divided into point feature and line feature. A keypoint extraction algorithm SIFT presented by David. G. Lowe which has been widely used in image registration [22]. Ballard DH presents a method that has line feature applied in image registration to detect particular shape in an image [23].

In side scan sonar images of underwater terrain, there are no significant keypoints. Side scan sonar images are often characterized by textured regions corresponding to different types of underwater terrain, so line feature is selected for triangle matching to improve the accuracy of image registration [24]. Thus, this paper presents a feature-based registration method, which uses Line Segment Detector (LSD) [25] to extract line features and constructs the triangular features to capture transformation information.

The main steps of the method are as follows: firstly, the original image is preprocessed before feature extraction; secondly, the LSD method is used to extract the line segment features from a pair of images, and these line segments are adaptively filtered to form triangular structure; thirdly, transformation parameters are calculated by using a pair of similar triangles; finally, image is transformed according to the transformation parameters to complete the registration and stitching of this image.

The rest of the paper is organized as follows: section 2 introduces the preprocessing operation and the method of line feature extraction; section 3 discusses the method for extracting and filtering line features; section 4 introduces the method of forming and matching triangles according to line features;

section 5 introduces image registration and stitching through transformation relations; section 6 shows the performance of the method and discusses some data in our experiment; section 7 summarizes the paper.

2 The Preprocessing of Sonar Image

Underwater sonar scan images store much useful information, such as pixel data, band information, geographic information and affine transformation data. In this section, according to the geographic information, a pair of images with the same geographic region can be intercepted for image registration.

In order to extracting good features for image registration, source and target images are smoothed off-noisy by Gaussian low-pass filter, where the standard deviation parameter σ of Gaussian is set to 5. Since both high frequency noise and edge information are weakened after smoothing, image stretching operation is introduced to enhance edge information, which is shown in Equation. (1).

$$I(x, y) = \frac{I(x, y) - I_{\max} \times L_{th}}{I_{\max} \times H_{th}} \times (V_{Max} - V_{Min}) \quad (1)$$

where I_{\max} is the maximum gray value of the original image, the V_{Max} and the V_{Min} are the standard gray value 255 and 0 respectively, L_{th} and H_{th} are the threshold for image stretching operation, which are set to 0.2 and 0.4 respectively in the experiments. An example of preprocess is shown in Fig.1. The intercepted region is the image to be registered, and target image will have the same operation.

3 Line Feature Extraction

3.1 Line Segment Detection

In this section, an effective line segment extraction (LSD) algorithm is selected to extract line features, which can capture line segment detection to result in a short time without parameter adjustment.

LSD algorithm starts with a Gaussian sampling for input image which scale s set to 0.8. The

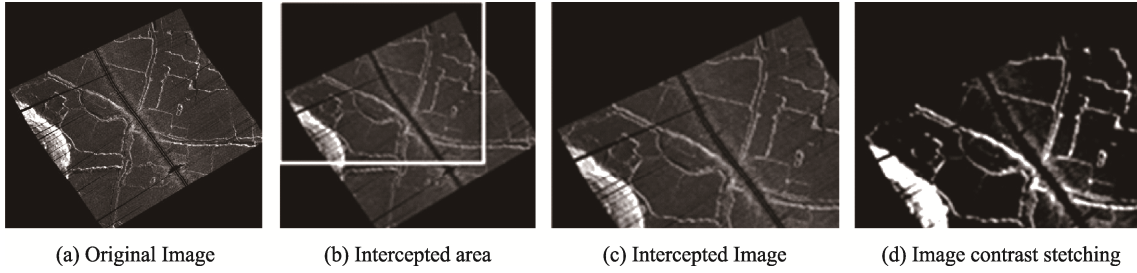


Fig.1 The Example of Preprocessing. (a) is the grayscale image of the source image, and (c) is the cropped part which is the rectangular area in (b) according to the geographic information from source image, (d) can be obtained by stretching.

gradient value and level-line angle of each point are calculated, and the angle tolerance is set to $\tau = \pi/8$, the probability that the horizontal line of a given point is aligned in a rectangle: $p = \tau/8 = 1/8$. According to the gradient value, all the points are sorted in descending order and are set to UNUSED, then the largest gradient point at the head of the state list is taken as the seed and the starting point. According to the direction of the gradient angle within the threshold $[-\tau, \tau]$ for regional diffusion, UNUSED points around the seed are filtered and set to USED, which called “aligned point”.

A series of adjacent points in the region are contained in a rectangular box r , which is the smallest rectangle that can contain the line-support region of these points. This rectangle can be regarded as a candidate line with length L_r , and the direction of the long axis of rectangle r is set as the direction of this line. The aligned points number is k in the smallest rectangle region, and the total number of points in the rectangle is n .

The number of false alarms (NFA) of this rectangular region is calculated to determine whether this rectangle can be regarded as a straight line. The NFA of rectangle r is defined by Equation. (2).

$$NFA(r) = N_{test} \cdot B(n, k, p) \quad (2)$$

$$N_{test} = (MN)^{5/2} \quad (3)$$

$$B(n, k, p) = \sum_{j=k}^n \binom{n}{j} p^j (1-p)^{n-j} \quad (4)$$

$$\binom{n}{j} = \frac{\Gamma(n+1)}{\Gamma(k+1) \cdot \Gamma(n-k+1)} \quad (5)$$

N_{test} is the number of candidate rectangles. The size of image is $M \times N$, thus the width of the rectangle is at most $(MN)^{1/2}$, and there are $(MN)^2$ potential line segments in this image, so the total number of possible rectangles is $(MN)^{5/2}$. $B(n, k, p)$ is the probability that the number of alignment points corresponding to the rectangle in noise model is not less than the number in actual model. Γ is the grade value of aligned points which level-line angle is decomposed into independent and uniformly random distribution.

The examples of line segment detection are shown in Fig.2. There are 1139 line segments detected from source image. From the above line segment image, there are a large number of short-length line segments gathered in some gray areas, and these segments are not conducive to the registration of this

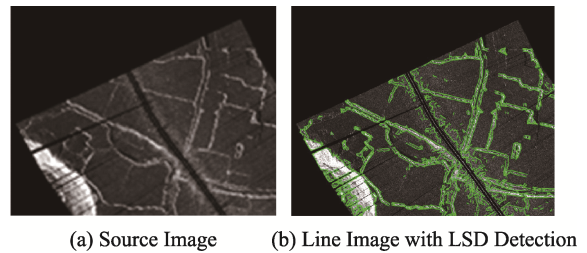


Fig.2 Line Feature Detected by the LSD Algorithm. (a) is the source image, (b) is the line image based on the segment coordinate data captured by LSD line detection of source image

image. Therefore, it is necessary to further filter the detected line segment, the work of line filtering is presented in the next section.

3.2 Line Segment Filtering

The segment features detected by the LSD algorithm can be filtered by the attention mechanism. First, morphological region filtering can be used to obtain the non-stray lines inside the image, then a portion of the segment can be removed by length saliency, and finally the approximately equal line segment features can be obtained by the similarity of the line segments.

3.2.1 Morphological Region Filtering

Depending on the brightness value, the grayscale image can be divided into three parts: the black background area, the white feature area and the gray area in an intermediate state. Theoretically, the line segment detected by LSD is located at the edge of the white area of the gray image. In the actual line segment detection image, it can be seen that short and messy line segments are located in the gray area, so it is necessary to filter these line segments to obtain spurious-free line segments. The algorithm of the gray area extraction is described in Algorithm 1.

In the Algorithm 1, \oplus is the dilation operation symbol, \ominus is the erosion operation symbol. $A_{5 \times 5}$, $B_{35 \times 35}$ and $C_{8 \times 8}$ are the computing kernels with size 5×5 , 35×35 and 8×8 respectively. The

area extracting steps are shown in Fig.4.

In the Fig.4, the white area in the obtained binary image is the collection of black background area and gray area in the gray image, the pixel value in the white background area is 1. The segments in the white background area will be filtered according to the sum of the pixel values in the 5×5 area centered on line endpoint. If the summation is not equal to zero, it means that the line segments are located in the white background area of binary image, and the line segments will be deleted.

3.2.2 Line Length Saliency Filtering

After region filtering, line segments can be adaptively restricted by line length saliency to further filter short line segments. Adaptive adjusting the threshold T_{len} of line segments length can avoid the problem that the line segments number is too small due to the length limitation in multiple filtering, which will reduce the accuracy of image registration and cracking.

3.2.3 Line Segment Similarity Filtering

After filtering by region and line length, the number of line segments is not equal. The number of line segments in the pair of images is almost equal through the similarity processing, so redundant line segments can be filtered by the similarity, which means that the line segments without similar line segments in another image will be removed.

The similarity of the segment is determined by

Algorithm1: Extract regions

INPUT : The gray image I_0 .
 PUTPUT: The binary image I_7 .

1 Binarization: $I_1(x, y) \leftarrow \begin{cases} 1 & I_0(x, y) > 5 \\ 0 & I_0(x, y) \leq 5 \end{cases}$

2 Close Operation1: $I_2 \leftarrow (I_1 \oplus A) \ominus A, A_{5 \times 5}$

3 Close Operation2: $I_3 \leftarrow (I_2 \oplus B) \ominus B, B_{35 \times 35}$

4 Xor: $I_4 \leftarrow \text{xor}(I_2, I_3)$ /*Extracting gray areas*/

5 Open Operation: $I_5 \leftarrow (I_4 \ominus C) \oplus C, C_{8 \times 8}$

6 Complement: $I_6(x, y) \leftarrow 1 - I_2(x, y)$

7 Or: $I_7 \leftarrow I_5 \mid I_6$ /*Add gray areas into the background*/

Fig.3 Algorithm1: Extract Regions

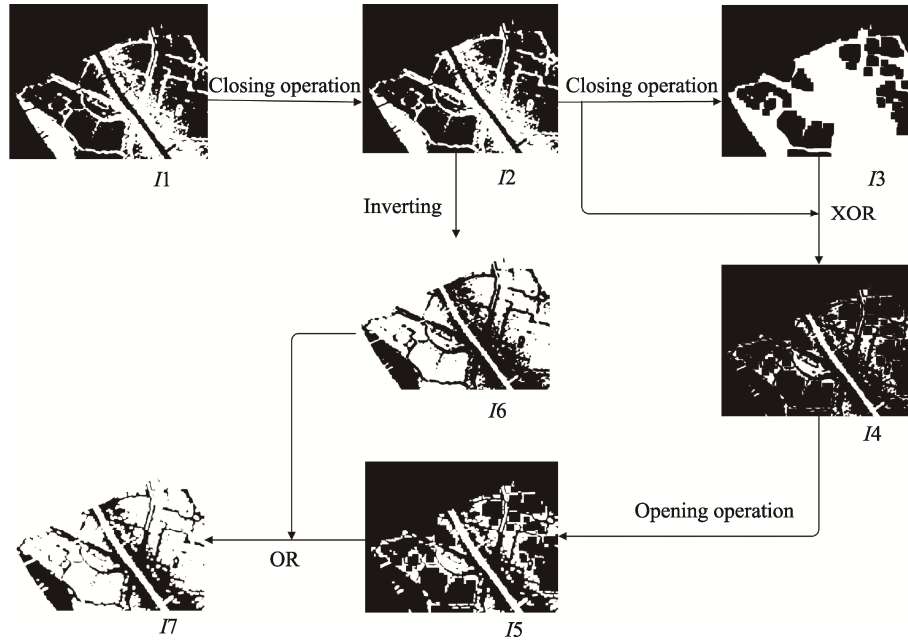


Fig.4 The Area Extraction Display

the length, angle and position. The angle difference between two line segments is calculated from the slope of line by using the least square method [26]. When the angle difference between the two line segments is less than the threshold $T_{\text{angle}} = \pi/36$, the two line segments are considered to be approximately parallel line segments. Through the comparison of length and position to get the similar line segments in the pair of images.

4 Triangle Matching

Through the heuristic greedy algorithm, the local optimal solution is found, then the feasible final solution is obtained which is the optimal transformation matrix [27]. First, there are similar line segment features that have been screened out, then similar triangle pairs are selected based on the length and angle of the line feature, finally the optimal transformation matrix is found from the vertices of the triangle.

4.1 The Composition of Triangle

A triangle can be determined by a side-line and two base-angles. In order to construct a triangle in an image, first a base-side is fixed, then two hypote-

nuses are selected to get two base-angles. The main steps are as follows:

(1) A line segment is selected as the reference of base-side, then two line segments are selected as the reference of hypotenuses.

(2) All selected line segments are extended or shortened to make them intersected, the vertex and the side length of triangle can be captured. At this time, the actual length of a side may become longer or shorter, especially when a side length become shorter. As a result, the side length may be less than the threshold value of line segment T_{len} of line segment length. It is necessary to re-judge whether the actual side length meets the threshold.

(3) From two selected hypotenuses and base-side to calculate the values of two base-angles. The two base-angles should be greater than the angle threshold T_{angle} to avoid the situation that the base-side is approximately parallel to thypotenuses. By a base-side and two base-angles of triangle, according to the principle that determining a triangle by two corners and a side. Candidate triangles are shown in Fig.5. There are 2454 triangles in the triangle image, and some triangles actually constructed out of image.

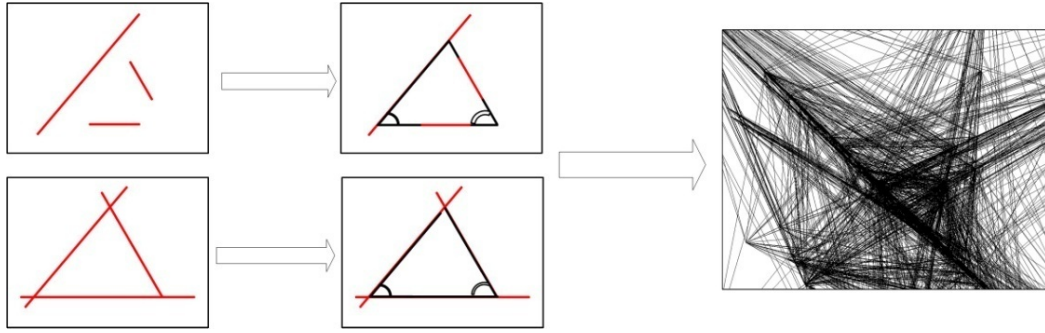


Fig.5 Schematic Diagram of Triangle Construction

4.2 Triangle Similarity Matching

In the procession of constructing triangles, triangles should be filtered according to the similarity. A triangle is selected in the source image as a reference triangle, the similar triangle will be found in another image. The similar triangles in target image can be found according to the following steps.

(1) A triangle is selected from source image as a reference triangle for target image. The base-side of this triangle is taken as the reference similarly base-side, and the two base-angles under the condition of this reference triangle base-side are updated as Equation. (6).

$$\begin{aligned}\theta_1 &= \theta_{\text{left}} - \theta_{\text{line}} \\ \theta_2 &= \theta_{\text{right}} - \theta_{\text{line}}\end{aligned}\quad (6)$$

where θ_1 and θ_2 are the updated values of target triangle base-angles, θ_{left} and θ_{right} are the base-angles of reference triangle, θ_{line} is the angle of candidate base-side line of a similar triangle in target image.

(2) Two line segments in the target image are taken as hypotenuses, with candidate base-side to calculating two base-angles θ_{1b} and θ_{2b} . These two angles are compared with θ_1 and θ_2 . If the difference between θ_1 and θ_{1b} , θ_2 and θ_{2b} is less than the angle threshold T_{angle} , these two line segments are considered as the similarly hypotenuse of reference triangle.

(3) These two hypotenuses and the candidate base-side in the target image are used to calculate the radius of triangle circumcircle. If the radius length difference between triangle in source and target image is less than T_{r_dif} , this pair of triangles are similar.

After triangle similarity processing, each triangle in target image has a similarly triangle in source image.

5 Registration and Stitching of Images

5.1 Image Registration

Through the previous process, triangles in these two images are obtained and matched, to find the optimal image affine transformation matrix ^[28] for image registration.

After similarly filtering, triangles can be used to calculate three-point affine transformation matrix H , which from the source image to the target image, and it is defined as Equation. (7).

$$H = \begin{bmatrix} a_1 & a_2 & t_x \\ a_3 & a_4 & t_y \\ 0 & 0 & 1 \end{bmatrix}\quad (7)$$

where (t_x, t_y) represents the translation, and the parameter $a_i, (i=1,2,3,4)$ reflects the rotation and scaling of the image.

After obtaining the affine transformation matrix H , it is necessary to perform filtering processing of migration and scale transformation. Among them,

the displacement limit and the zoom difference limit are as follows:

$$|t_x| < b_{\text{limit}} \text{ and } |t_y| < b_{\text{limit}} \quad (8)$$

$$\begin{cases} |a_1|^2 + |a_2|^2 - 1 < k_{\text{limit}} \\ |a_3|^2 + |a_4|^2 - 1 < k_{\text{limit}} \end{cases} \quad (9)$$

The offset threshold $b_{\text{limit}}=10$ and the scaling difference threshold $k_{\text{limit}}=0.2$ are all empirical values. These thresholds are used to make sure that the transformation matrix is calculated from two triangles with a certain degree of similarity. The transformed line segment image is compared with the line segment image of target image to obtain the Pearson Correlation Coefficient (PCC) ^[29] of these two images.

$$L_{\text{corcoef}} = \frac{\sum_i (a_i - \bar{a}) \sum_i (b_i - \bar{b})}{\sqrt{\sum_i (a_i - \bar{a})^2} \sqrt{\sum_i (b_i - \bar{b})^2}} \quad (10)$$

where a_i is the value of pixel i in source image, b_i is the value of pixel i in target image, \bar{a} is the average pixel value of source image, \bar{b} is the average pixel value of target image, and L_{corcoef} is the correlation coefficient about the line feature image of this pair images.

Each pair of triangles is used to calculate line image similarity, and filter the transformation matrix H of a pair of triangles with the greatest similarity value.

5.2 Image Stitching

The new coordinates in fusion-image are needed to perform coordinate transformation. The equations are defined as Equation. (11).

$$\begin{cases} x'_{1i} = x_{1i} + re_{10} + X_{\text{off}1} \\ y'_{1i} = y_{1i} + re_{11} + Y_{\text{off}1} \\ x'_{2i} = x_{2i} + re_{20} + X_{\text{off}2} \\ y'_{2i} = y_{2i} + re_{21} + Y_{\text{off}2} \end{cases} \quad (11)$$

(x_{1i}, y_{1i}) , $i=1,2,3$ and (x_{2i}, y_{2i}) , $i=1,2,3$ are the coordinates of triangle vertices in source and

target images respectively, (x'_{1i}, y'_{1i}) , $i=1,2,3$ and (x'_{2i}, y'_{2i}) , $i=1,2,3$ are the updated coordinates in fusion-images respectively. (re_{10}, re_{11}) and (re_{20}, re_{21}) are the offsets from the cropped image to the full size image respectively according to the geographic information, $(X_{\text{off}1}, Y_{\text{off}1})$ and $(X_{\text{off}2}, Y_{\text{off}2})$ are the offsets from these full size image to fusion image respectively.

According to (x'_{1i}, y'_{1i}) and (x'_{2i}, y'_{2i}) , a three-point transformation matrix M from source image to fusion-image can be calculated. The flowchart of this process is shown in Fig.6.

By affine transformation of source image with matrix M to obtain $It1$ in the fusion-image space, as shown in Fig.7(b). At the same time, target image is embedded in an empty image of the same size as the fusion image to obtain the $It2$, as shown in Fig.7(d). These two images are the same size of (row, col), so that image fusion can be performed directly.

The transformed image is processed, three partial mask images (a), (b) and (c) can be captured by logical operation and shown in Fig.8. These three image parts IM_1 , IM_2 and IM_3 in the source and target image are extracted by the mask Im_i , ($i=1,2,3$) respectively. The overlapped part is the weighted average of the extracted two transformed images. The resulting image section is shown in Fig.8(d), (e) and (f). Finally, these three parts are superimposed into the final fusion image to obtain the image mosaic result.

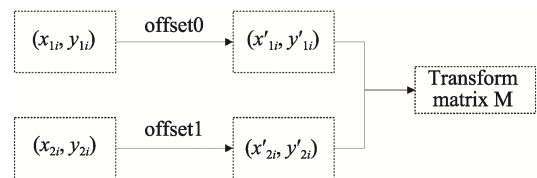


Fig.6 Coordinate Transformation and Transformation Matrix Flowchart

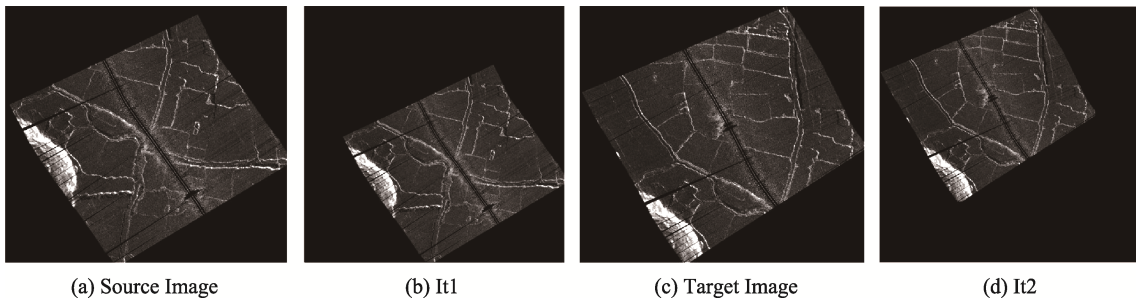


Fig.7 Transform Source and Target Image into a Collection Coordinate System. (a) source image in the original coordinate system, (b) $It1$ in the transformed coordinate system, (c) target image in the original coordinate system, (d) $It2$ in the transformed coordinate system.

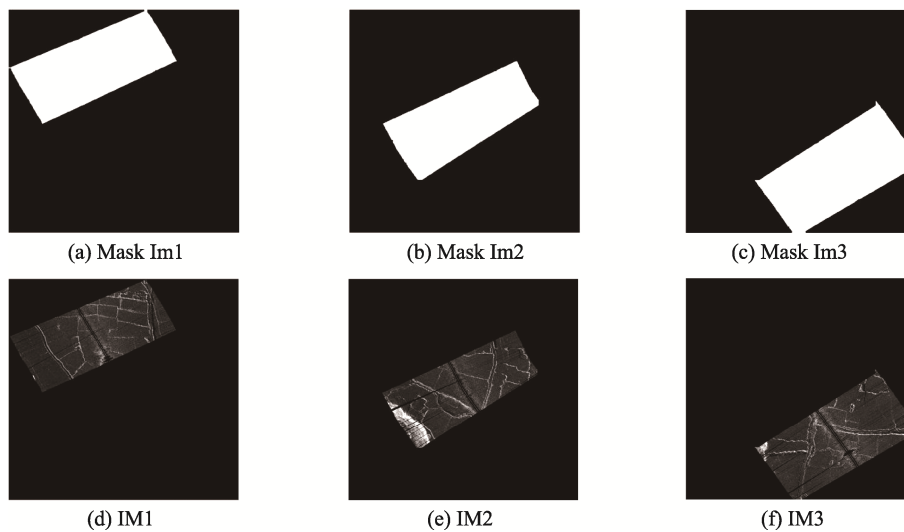


Fig.8 Mask Image. (a), (b) and (c) is mask image of each part; (d), (e) and (f) is based on the part of the image obtained by the mask.

6 Experimental Results

6.1 Experimental Environment

The platform is the Dell T5820 image workstation: the operating system is windows 10, Intel Xeon w2123 CPU @ 3.6 GHz, and the memory is 8 GB. The algorithm is implemented by compiling Python code through visual studio 2015 compilation platform.

6.2 Comparison of Image Stitching

multiple sets of data are tested in this experiment, in order to facilitate display in the article, five sets of image data are selected for display, and the method is compared with the traditional SIFT fea-

ture-point-based method. The testing results of these two methods are as follows.

The image is divided into five rows and each row has four columns. The first column is the stitched image using triangle matching, the third column is the stitched image of the sift method, the second and fourth columns are the enlarged part of the red area in the left image. The green rectangle is the area where the stitching results of the two methods are obviously different. From the result of image stitching, both methods can be used for sonar image stitching, but the effect of triangle matching method is better. After zooming in the stitching area, it is clear that the image stitched by the sift method has obvious gap near the stitching edge.

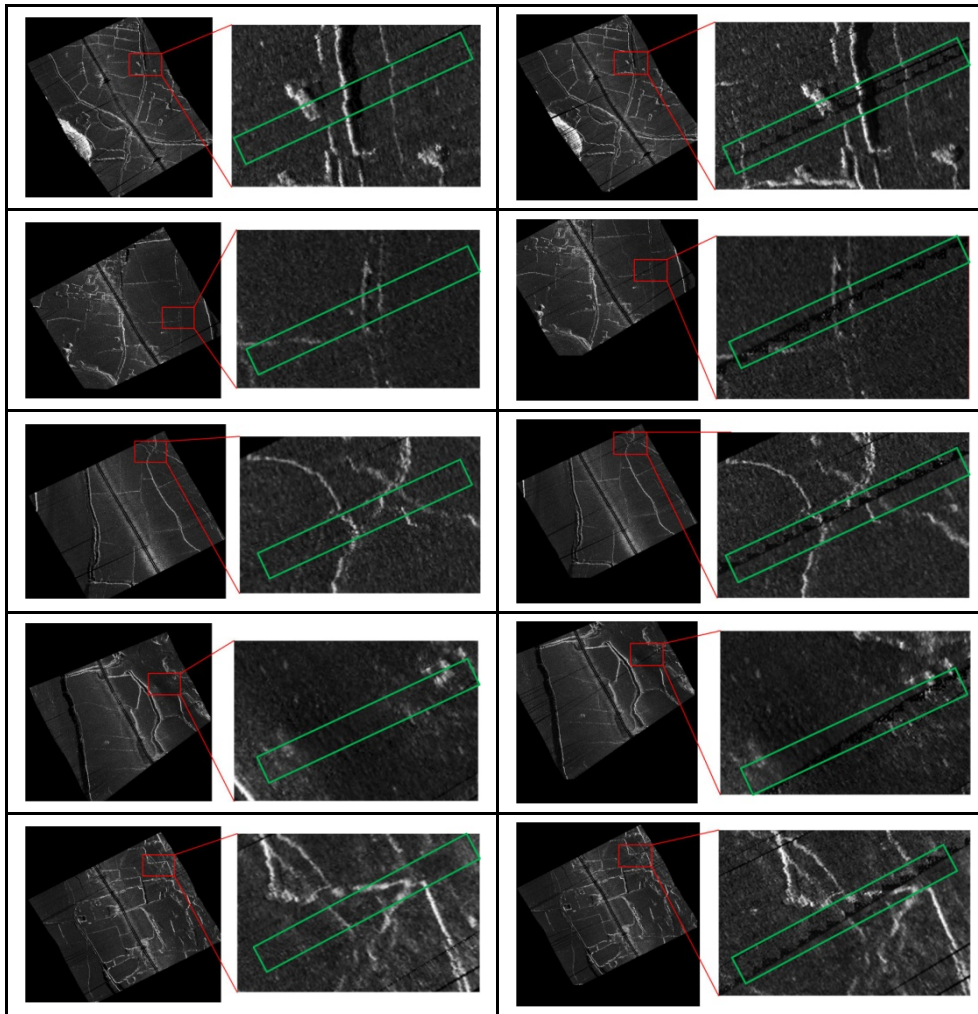


Fig.9 Image Stitching Results.

6.3 Feature Region Screening Performance Analysis

This experiment shows the performance of the area filtering processing algorithm on five pairs of images. The processing time consumed by processing five groups of images is shown in Table I.

The experimental results data in Table 1 prove that the running time can be reduced by 90.07s, 36.03s, 27.43s, 73.19s and 104.22s respectively, under the different conditions of filtering procession in characteristic areas. The average lift code processing time is 66.18s, and the reduced time is related to the number of segments detected in the actual test.

6.4 Line Segments Filtering Operation

The number of line segment features detected by the LSD algorithm can be reduced by filtering based on region, length and similarity. The effectiveness of this process is shown in Fig.10.

In this experiment, there are five groups images in the test methods, every two rows are a group in Fig.10. There are five columns in each row, the first column is the original grayscale image, the second column is the detected line segment image, the third column is the regional filtered image, the fourth column is the length processed image, and the fifth column is the similarity filtered Image. After a series of processing, the same number of segments is

captured. The number of line segments changes as shown in Table 2 and Fig.11.

From the line chart of line segments number in Fig.11, it can be seen that after a series of filtering processions, the mean in the number of line segments are 868, 241, 41 and 16. By reducing the number of line segments through line segment filtering, the efficiency of subsequent feature processing can be improved. It is clear that the processing improves the efficiency of subsequent feature processing.

6.5 Triangle Similarity Operation

The number of triangles in source and target image are counted in thousands, for the calculation of the conversion matrix, the number is large, it is

necessary to filter these triangles. These triangles are filtered by angle and line length, and the triangles image and number changes are shown in Fig.12 and Table 3 respectively.

The triangle image is divided into five rows and each row has four columns. The first and the third columns are the detected triangle images, and the second and the fourth columns are the filtered triangle images. In the actual constructed triangles, there are some triangles exceed the image effective area. After triangle similarity procession, the number of triangles dropped by an order of magnitude, and all the triangles in target image have similar triangles in source image. It is clear that the computation of transformation matrix is decreased for this number of triangles.

Table 1 Performance Analysis of Region Filtering

Pairs	Region Screening (s)	No Region Screening (s)	Time Difference (s)
A	27.16	117.23	90.07
B	14.14	50.17	36.03
C	16.25	43.68	27.43
D	13.22	86.41	73.19
E	15.44	119.66	104.22

Table 2 Trend of Line Segments Number

Pairs	Detection	Region	Length	Similarity
A	1043	147	47	16
	1139	138	43	16
B	482	82	31	14
	800	94	43	14
C	525	266	38	16
	901	367	55	16
D	617	120	32	14
	609	128	34	14
E	1321	547	44	20
	1185	524	45	20
Mean	868	241	41	16

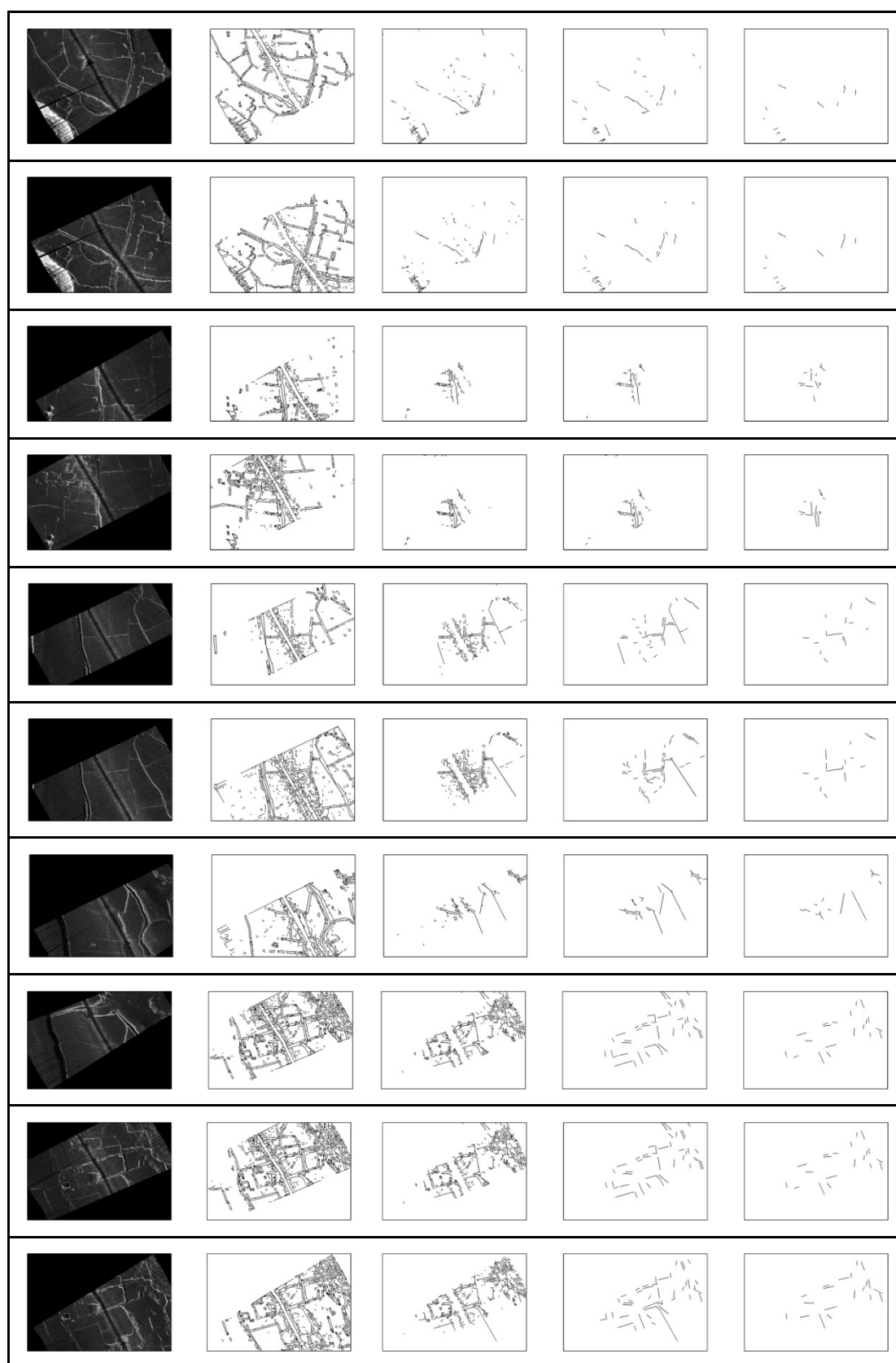


Fig.10 Image of the Changes of the Number of Line Segments

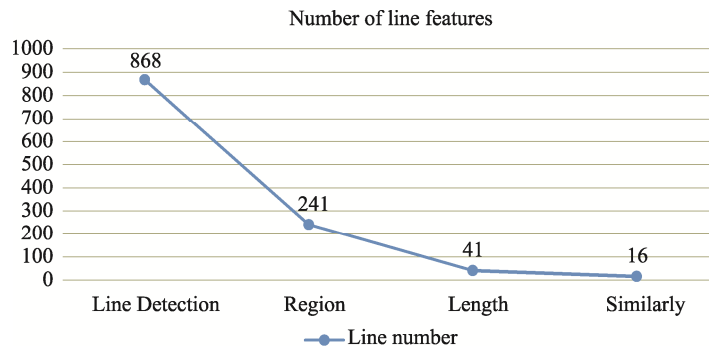


Fig.11 The Trend Graph of the Line Segments Mean Number

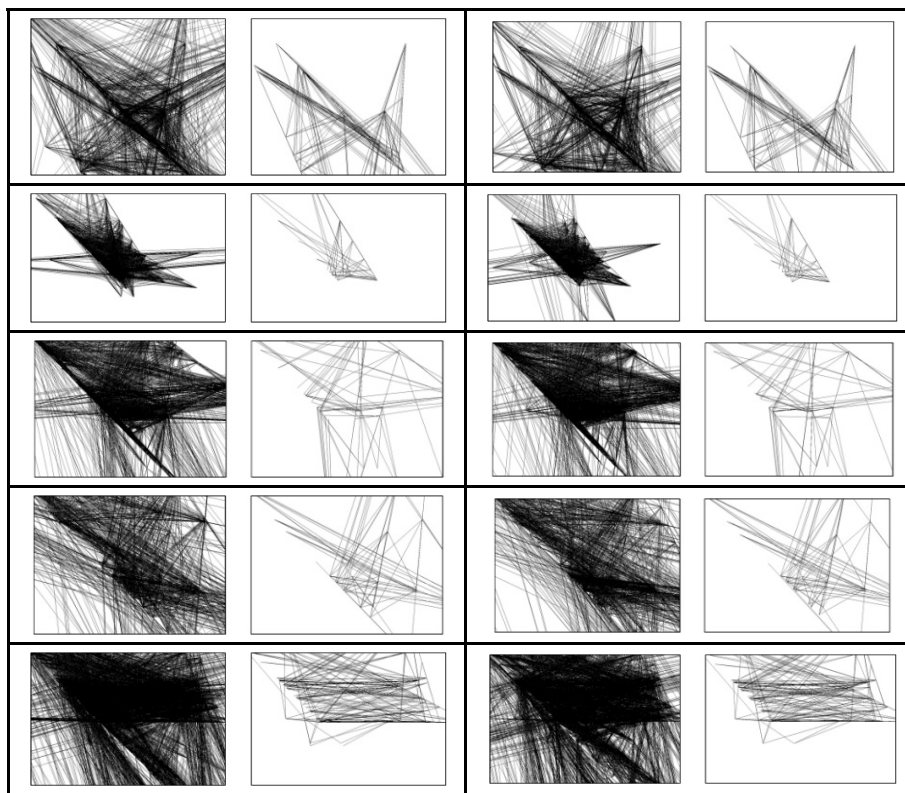


Fig.12 Triangles Image with Similarity Processed

Table 3 Triangle Number

Pairs	Triangle 1	Filtered	Triangle 2	Filtered
A	2454	162	2397	162
B	1582	26	1448	26
C	2416	54	2498	54
D	1542	54	1720	54
E	5116	158	4562	168

7 Discussion

Through comprehensive comparison and analysis with other methods, proposed triangle image registration and stitching based on line features are effective. The method of image registration base on line features, which can cleverly avoid the inconspicuous features of sonar image keypoints. As shown in Fig.13 below, the line feature method is used to process these images, the line feature can better describe the contour of the underwater terrain. For the image to extract keypoints, it can be seen that the number of keypoints on the image is small, which cannot describe the whole sonar image well. The proposed triangle registration method based on line feature can make good use of the visual saliency of image features to depict the underwater terrain in the image. The three principles of filtering based on attention mechanism are adopted in the process of screening the characteristics of the line segment, which remove some stray segment features by using the significance and morphological filtering of the segments, the strength of the similarity of line segment features

used to filter and retain similar line features, these processing play an important role in improving the calculation accuracy.

In the process of triangle matching, the heuristic greedy algorithm is used to calculate the solution of each part, then get a feasible final solution. The points, lines and angles of the triangles are similarly filtered respectively to obtain similar triangles, after that the image transformation matrix is obtained, then the image is stitched after the transformation.

Because of a heuristic greedy algorithm is used in the selection of triangles, a lot of calculation is needed in the running of the program, which makes the program unable to achieve the real-time. In the future research, the adjustment of data structure, the optimization of filtering methods, and the application of some other algorithms can improve the efficiency of triangle filtering, so as to obtain the corner point information of the triangle more quickly to calculate the transformation matrix. The method proposed in this paper is mainly aimed at the sonar image's alignment, line features are used to describe the image, and then the

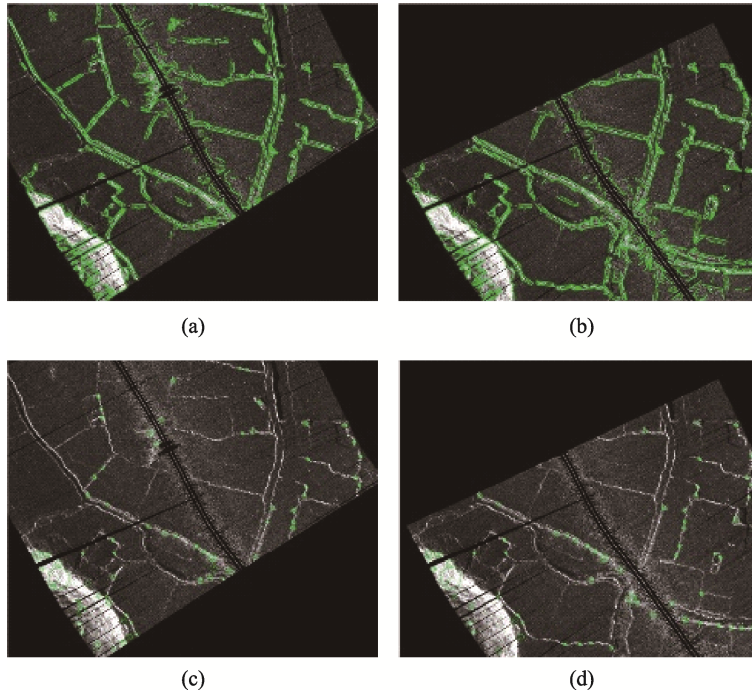


Fig.13 The Image of Line Features and Keypoints Respectively. (a) and (b) are the line feature image, (c) and (d) are the image of keypoints.

transformation matrix is obtained for image matching and stitching. The line feature method can be combined with the point feature method. In addition, non-manual features, such as those extracted by deep learning methods, can be used in this problem to improve the robustness of the algorithm.

In summary, the proposed method has better performance on images with insignificant keypoints. Therefore, it has a higher application value and can be applied into more fields, such as lane detection for autonomous driving^[30] and image processing for aerospace field^[31].

8 Summary

Aiming at registering and stitching the sonar scan images of underwater terrain, this paper proposes an effective method based on triangle matching. The linear terrain features in the underwater sonar image are relatively obvious, and this type of image can be registered and stitched using a method based on line features. Therefore, this method uses LSD to detect line features of the image, then these lines are processed by similarity to form triangles. The relative angle, segment length and relative position are combined to obtain transformation matrix for image transformation, finally the matrix is used to stitch and merge the images. From the actual image stitching results in this paper, it is not visible to the naked eye splicing gaps. The linear feature method can be used to improve the accuracy of image registration by making good use of the linear features protruding from the underwater terrain. However, due to the use of line features for screening, the program cannot meet the requirements of real-time processing, so the algorithm needs to be improved later to shorten the program running time.

References

- [1] Jan Petrich, Mark F. Brown, Jesse L. Pentzer, John P. Sustersic, Side scan sonar based self-localization for small Autonomous Underwater Vehicles, *Ocean Engineering*, Volume 161, 2018, Pages 221-226.
- [2] Isabelle Leblond, Sébastien Tavvry, and Marc Pinto, Sonar image registration for swarm AUVs navigation: Results from SWARMS project, *Journal of Computational Science*, Volume 36, 2019, 101021.
- [3] M.N.V.S.S. Kumar, G.S.B. Rao, L. Ganesh, R.Goswami, Expectation–Maximization Based Image Fusion Algorithm for Detection of Underwater Targets from SONAR Images, *Procedia Computer Science*, Volume 85, 2016, Pages 782-789.
- [4] Y. Han, C. Zheng, D. Sun, Signal design for underwater acoustic positioning systems based on orthogonal waveforms, *Ocean Engineering*, Volume 117, 2016, Pages 15-21.
- [5] Monica Montefalcone, Alessio Rovere, Valeriano Parravicini, Giancarlo Albertelli, Carla Morri, Carlo Nike Bianchi, Evaluating change in seagrass meadows: A time-framed comparison of Side Scan Sonar maps, *Aquatic Botany*, Volume 104, 2013, Pages 204-212.
- [6] Geraeds M, van Emmerik T, de Vries R, bin Ab Razak MS. Riverine Plastic Litter Monitoring Using Unmanned Aerial Vehicles (UAVs). *Remote Sensing*. 2019; 11(17): 2045.
- [7] S. Song, Y. Li, Z. Li, et al, Seabed Terrain 3D Reconstruction Using 2D Forward-Looking Sonar: A Sea-Trial Report from The Pipeline Burying, *IFAC-PapersOnLine*, Volume 52, Issue 21, 2019, Pages 175-180.
- [8] Hangil Joe, Jason Kim, Son-Cheol Yu, Sensor Fusion-based 3D Reconstruction by Two Sonar Devices for Seabed Mapping, *IFAC-PapersOnline*, Volume 52, Issue 21, 2019, Pages 169-174.
- [9] Dong C, Liu J, Xu F, Liu C. Ship Detection from Optical Remote Sensing Images Using Multi-Scale Analysis and Fourier HOG Descriptor. *Remote Sensing*. 2019; 11(13): 1529.
- [10] M. Zhao, X. Zhang, Q. Yang, Modified Multi-Mode Target Tracker for High-Frequency Surface Wave Radar. *Remote Sens*. 2018, 10, 1061.
- [11] Ahmet Gunes, Mehmet B. Guldogan, Joint underwater target detection and tracking with the Bernoulli filter using an acoustic vector sensor, *Digital Signal Processing*, Volume 48, 2016, Pages 246-258, ISSN 1051-2004.
- [12] R. Liu, D. Wang, P. Jia, H. Sun H, An Omnidirectional Morphological Method for Aerial Point Target Detection Based on Infrared Dual-Band Model. *Remote Sensing*. 2018; 10(7): 1054.
- [13] C. Rao, K. Mukherjee, S. Gupta, et al, Underwater mine detection using symbolic pattern analysis of sidescan sonar images, 2009 American Control Conference, St. Louis, MO, 2009, pp. 5416-5421.
- [14] B. Lucas and T. Kanade. An iterative image registration

- technique with an application to stereo vision. In Proceedings of the International Joint Conference on Artificial Intelligence, Vancouver, Canada, 1981: 121-130.
- [15] D. I. Barnea, H. F. Silverman, A Class of Algorithms for Fast Digital Image Registration, *Computers*, vol. C-21, no. 2, pp. 179-186, Feb. 1972.
- [16] P. E. Anuta, Spatial Registration of Multispectral and Multitemporal Digital Imagery Using Fast Fourier Transform Techniques, *Geoscience Electronics*, vol. 8, no. 4, pp. 353-368, Oct. 1970.
- [17] Neto VFDC, Campos MFM, An Improved Methodology for Image Feature Matching// XXII Brazilian Symposium on Computer Graphics & Image Processing. *Computer Society*, 2009.
- [18] X. Zhang, D. Ma, H. Yu, Y. Huang, P. Howell, B. Stevens, Scene perception guided crowd anomaly detection, *Neuro computing*, 2020.
- [19] J.P.W. Pluim, J.B.A. Maintz and M.A. Viergever, Mutual-information-based registration of medical images: a survey, *Medical Imaging*, vol. 22, no. 8, pp. 986-1004, Aug. 2003.
- [20] Zahra Hossein-Nejad, Mehdi Nasri, A-RANSAC: Adaptive random sample consensus method in multimodal retinal image registration, *Biomedical Signal Processing and Control*, Volume 45, 2018, Pages 325-338.
- [21] Yuan C, Clarence W. DE SILVA, Bing L, Liqun W, Ziwen W, Application of Feature Extraction through Convolution Neural Networks and SVM Classifier for Robust Grading of Apples. *Instrumentation*, 2019, 6(4): 59-71.
- [22] David. G. Lowe. Distictive Image Features from Scale-Invariant Keypoints. *the International Journal of Computer Vision*. 2004, Vol.60(2). 91-110.
- [23] Ballard D. H. Generalizing the Hough transform to detect arbitrary shapes. *Pattern Recognition*, 1981, 13(2): 111-122.
- [24] M. Lianantonakis, Y. R. Petillot, Sidescan Sonar Segmentation Using Texture Descriptors and Active Contours, *Journal of Oceanic Engineering*, vol. 32, no. 3, pp. 744-752, July 2007.
- [25] Grompone von Gioi Rafael, Jakubowicz Jérémie, Morel Jean-Michel, Randall Gregory. LSD: a fast line segment detector with a false detection control. *Pattern Analysis and Machine Intelligence*, 2010, 32(4).
- [26] D. G. Lowe, "Object recognition from local scale-invariant features, the Seventh IEEE International Conference, Kerkyra, Greece, 1999, pp. 1150-1157 vol.2.
- [27] S. Hussain, Greedy heuristics for minimization of number of terminal nodes in decision trees, *Granular Computing*, Noboribetsu, 2014, pp. 112-115.
- [28] L. Vincent, Morphological grayscale reconstruction in image analysis: applications and efficient algorithms. *Image Processing*, vol. 2, no. 2, pp. 176-201, 1993.
- [29] A. M. Neto, A. C. Victorino, I. Fantoni, D. E. Zampieri, J. V. Ferreira and D. A. Lima, Image processing using Pearson's correlation coefficient: Applications on autonomous robotics, *Autonomous Robot Systems*, Lisbon, 2013, pp. 1-6.
- [30] Minh, Hoang Toan, et al. Road Lane Detection Robust to Shadows Based on a Fuzzy System Using a Visible Light Camera Sensor. *Sensors* (Basel, Switzerland) 17.11(2017): 2475.
- [31] Liu Z, Zhang B, Li P, et al. Automatic registration between remote sensing image and vector data based on line features. *International Conference on Geo informatics*, 2011: 1-5.

Author Biographies



GUO Chunsheng, received his B.Sc. in Radio Engineering from the Northeastern University (NEU), Shenyang, China, and received a Ph.D. in Communication and Information System from the Nanjing University of Aeronautics and Astronautics (NUAA), Nanjing, China, in 1993 and 2002, respectively. He is currently an associate professor at the School of Communication Engineering, Hangzhou Dianzi University, China. His research interests are image segmentation and analysis, video moving objects detection, pattern recognition and Video anomaly detection.

Email: gcs@hdu.edu.cn



ZHANG Xuguang, received the B.S. degree in Electrical Technology from Northeast Normal University, and Ph.D. in Machinery and electronics engineering from Changchun Institute of Optics, Fine Mechanics and Physics, Chinese Academy of Sciences, China, in 2000 and 2008 respectively. He was a professor at the school of electrical engineering at the Yanshan University, China. He is currently a professor at the School of Communication Engineering, Hangzhou Di-

anzi University, China. His research interests include video and image processing, crowd behavior analysis and human behavior understanding.

Email: zhangxg@hdu.edu.cn



FANG Yinfeng, (S'12–M'15) received the Ph.D. Degree in computer science from the University of Portsmouth, Portsmouth, U.K., in 2015. He was a Postdoctoral Researcher in the Intelligent System and Biomedical Robotics Group for three years in University of Portsmouth. He is now an associate professor of Computer Science with the School of Communication Engineering, Hangzhou Dianzi University. He has authored and co-authored more than 30 peer-reviewed international journal and conference papers. His research interests include bioelectric signals acquisition electronics, signal processing, artificial intelligence algorithms and

neuromuscular rehabilitation.

Email: yinfeng.fang@hdu.edu.cn



WANG Yuxi, received the Ph.D. degree in optical engineering from Beijing Institute of Technology, Beijing, China, in 2018. She is now a lecturer in the School of Communication Engineering, Hangzhou Dianzi University. Her research interests include computer vision and augmented reality.

Email: yxwang@hdu.edu.cn



LIU Tao, is studying for a M.Sc. degree in the School of Communication Engineering, Hangzhou Dianzi University. His research interests include Video analysis and image processing.

Email: tao@hdu.edu.cn



Copyright: © 2020 by the authors. This article is licensed under a Creative Commons Attribution 4.0 International License (CC BY) license (<https://creativecommons.org/licenses/by/4.0/>).